

Scaling of $1/f$ noise in tunable break junctions

ZhengMing Wu, SongMei Wu, S. Oberholzer, M. Steinacher, M. Calame, and C. Schönenberger*

Departement für Physik, Universität Basel, Klingelbergstrasse 82, CH-4056 Basel, Switzerland

(Received 28 September 2008; revised manuscript received 16 November 2008; published 15 December 2008)

We have studied the $1/f$ voltage noise of gold nanocontacts in electromigrated and mechanically controlled break junctions having resistance values R that can be tuned from $10\ \Omega$ (many channels) to $10\ \text{k}\Omega$ (single-atom contact). The noise is caused by resistance fluctuations as evidenced by the $S_V \propto V^2$ dependence of the power-spectral density S_V on the applied dc voltage V . As a function of R the normalized noise S_V/V^2 shows a pronounced crossover from $\propto R^3$ for low-Ohmic junctions to $\propto R^{1.5}$ for high-Ohmic ones. The measured powers of 3 and 1.5 are in agreement with $1/f$ noise generated in the bulk and reflect the transition from diffusive to ballistic transport.

DOI: 10.1103/PhysRevB.78.235421

PACS number(s): 72.70.+m, 73.63.Rt, 73.40.Cg, 85.40.Qx

I. INTRODUCTION

The study of fluctuations (noise) in physical properties of condensed matter has been an active area of research for decades and has led to profound insights into time-dependent physical phenomena.^{1–5} In case of charge transport, the noise shows up as a fluctuating time-dependent ac voltage δV over the device with resistance R . The most generic noise contributions stem from equilibrium thermal fluctuations of the electron bath (Johnson-Nyquist noise),^{6,7} nonequilibrium shot noise caused by the granularity of charge,⁸ and resistance fluctuations.^{9–18} Whereas thermal and shot noises are frequency independent, resistance fluctuations display a strong dependence which often closely follows a $1/f$ relation over a large frequency range. Because of the $1/f$ dependence, this noise contribution dominates over thermal and shot noises at lower frequencies. $1/f$ noise has intensively been studied for bulk and thin-film conductors,^{9–18} in particular as a diagnostic tool for the technologically relevant electromigration (EM) mechanism.^{19–22} Noise at low and high frequencies has also been explored in small constrictions,^{23–26} nanoelectronic devices,^{27,28} quantum point contacts,²⁹ submicron interconnects,^{30,31} quantum coherent, quasiballistic and ballistic nanowires,^{32–39} and tunneling contacts.^{40,41}

The power-spectral density of resistance fluctuations S_R can phenomenologically be described by Hooge's law,^{9,12}

$$S_R(f)/R^2 = \frac{\alpha}{Nf}, \quad (1)$$

expressing proportionality of S_R with a $1/f$ frequency dependence. The proportionality factor α/N is ascribed to a material parameter α containing the strength of elastic and inelastic scatterings, on the one hand, and to an extensive variable N , on the other hand. The constant N denotes the number of statistically independent fluctuators in the volume. It is straightforward to derive this N dependence by assuming a resistance network with N resistors in series (or in parallel), all fluctuating independently. The total square fluctuation is then inversely proportional to N . In bulk conductors, the total number of electrons has been used for the variable N .^{12,15,42} Partial support for this view comes from semiconductors in which the carrier density can be changed over many orders of magnitude.^{42–44} Hooge's law therefore states that $1/f$

noise is a bulk phenomenon, originating homogeneously over the whole volume. In structures of reduced dimensionality, such as thin films and nanowires, where the surface may dominate over the bulk, the leading contribution to $1/f$ noise may stem from surface roughness and its fluctuations.^{9,45–47} The validity of bulk scaling of S_R has therefore been questioned. However, there are no quantitative studies on the scaling behavior of $1/f$ noise in nanocontacts with tunable cross sections in which this dependence could be explored.

In this paper we report on $1/f$ noise measured in tunable metallic nanoconstrictions obtained through EM (Ref. 48) and mechanically controlled break junctions (MCBJs).^{49–51} Our emphasis is on the role of the scaling parameter N in nanocontacts in the regime of few transport channels where the transition from diffusive to ballistic transport takes place. This transition is observed in our experiments at room temperature and we demonstrate that even in nanocontacts with only a few transport channels, $1/f$ noise is a bulk property.

II. EXPERIMENTAL SETUP AND CALIBRATION

Representative examples of EM junctions and MCBJs are shown in Figs. 1(a) and 1(b). They are both fabricated using electron-beam lithography and metal deposition in a lift-off process. In both cases Au wires with narrow constrictions with typical dimensions of 200 nm in length and 100 nm in width are defined first. Each wire has four terminals enabling the accurate measurement of the electrical resistance. Au wires are fabricated on oxidized (400 nm) Si substrates for EM junctions and on a flexible substrate for MCBJs, onto which a several micrometer thick insulating polyimide layer is cast.⁵³ To form an EM junction the four terminals are used in an automatic feedback-controlled EM process which continuously shrinks the wire constriction down to an atom-sized nanojunction as seen in Fig. 1(a).⁵² In MCBJs the wire constriction is first transferred into a suspended bridge by etching the underlying polyimide layer in an oxygen plasma as seen in Fig. 1(b). By bending the substrate the constriction can be narrowed in a controlled manner.^{49–51}

Before narrowing the constrictions, the as-fabricated devices have a junction resistance R_J of around $1\text{--}10\ \Omega$ at room temperature as determined in a four-terminal setup. The two-terminal resistance $R=R_J+2R_L$, which includes the

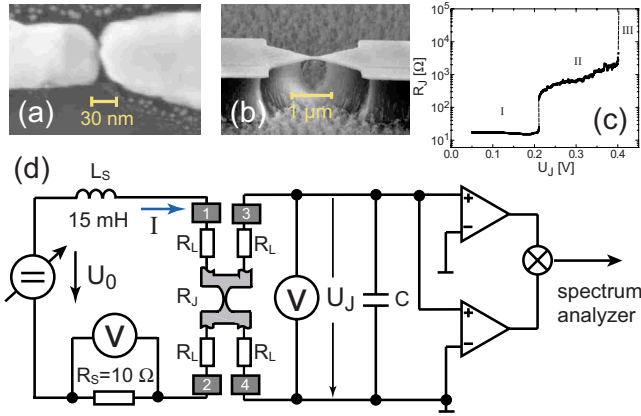


FIG. 1. (Color online) SEM images of (a) an EM junction and (b) a suspended bridge device used in the MCBJ setup. Panel (c) shows a characteristic EM induced evolution of the junction resistance R_J as a function of applied junction voltage U_J . Electromigration narrows the junction cross section in regime II (Ref. 52). Panel (d) shows schematics of the electric circuit used to measure the noise. R_L denotes the resistance of each lead in the four-terminal setup and C summarizes the total capacitance of the preamplifier and the connecting cables. The inductor L_S is used to separate the ac-noise measurement on the right from the dc biasing on the left.

lead resistance R_L on both sides, amounts to as much as 250 Ω . Because $R_L \gg R_J$ in virgin devices, the feedback-controlled process is mandatory to initiate a nondestructive narrowing by EM.^{52,54} In voltage-biased controlled EM, in which the voltage over the junction is stabilized by a fast analog feedback,⁵² narrowing sets in at a voltage of ≥ 0.2 V. The junction resistance R_J then rapidly evolves from a few ohms to ≈ 100 Ω . In this regime of active EM, R_J can further be increased into the k Ω regime by increasing the junction voltage. An example of this process is shown in Fig. 1(c). We emphasize that we do not measure the noise while EM proceeds. After narrowing the constriction at a “large” voltage, we switch the applied voltage back to values ≤ 0.2 V. During noise measurements, the junctions remain stable. In contrast to EM junctions, MCBJs have the advantage in that the junction size can be changed with an independent control parameter by mechanical bending. This allows changing the junction diameter while monitoring noise simultaneously.

We perform noise measurement in a four-terminal setup schematically shown in Fig. 1(d). An adjustable low-noise dc voltage source U_0 is connected via a series inductor L_S and a series resistor R_S to contacts 1 and 2 on the left side, driving a dc bias current I through the junction. $R_S = 10$ Ω is used to measure I and $L_S = 15$ mH serves to decouple ac from dc. The impedance of the inductor prohibits the shunting of the ac voltage fluctuations (noise). This only works if $\omega L_S > R_J$ (ω is the angular frequency $= 2\pi f$), defining a lower cutoff for the useful frequency window. The frequency-dependent noise is simultaneously measured on terminals 3 and 4 and fed into two low-noise preamplifiers (EG&G5184) and a spectrum analyzer (HP89410A). Here, the effective input capacitance C is diminishing the signal at high frequencies, defining an upper cutoff for the frequency window through the relation $1/\omega C > R_J$. For a typical junction resistance R_J

of 100 Ω and effective capacitance $C \approx 1$ nF, the useful frequency window spans approximately 3 orders of magnitude, i.e., 1 kHz $< f < 1$ MHz. We describe the f dependence of the circuit analytically (see below) and use this model to fit the total capacitance which contains parts of the Si chip, the connecting wires, and the amplifiers. When measuring noise, the two preamplifiers measure the same fluctuating signal in parallel. The spectrum analyzer is operated in the cross-spectrum mode and determines the Fourier transform of the cross-correlation signal from the two amplifiers,

$$S_V(f) := 2 \int_{-\infty}^{\infty} e^{i2\pi f t} \langle \delta U_1(t + \tau) \delta U_2(\tau) \rangle_{\tau} dt, \quad (2)$$

where $\delta U_{1,2}(t)$ denotes the time-dependent deviations from the average value of the junction voltage U_J measured on amplifiers 1 and 2, and $\langle \dots \rangle_{\tau}$ refers to averaging over τ . This signal is equivalent to the voltage power-noise spectral density. The correlation techniques can eliminate the voltage noises originating from the two amplifiers because the two amplifiers are independent.

All measurements are done at room temperature ($T = 300$ K) and thermal noise is used to calibrate the setup. The thermal noise of a resistor of value R is given by $S_V = 4kTR$. Due to the f -dependent elements in the circuit and the preamplifiers, the noise signal is in general attenuated. The attenuation factor A has two components $A = A_1 \times A_2$. A_1 is determined by the two circuits in Fig. 1(d) parallel to R_J : the one with the inductor L on the left and the one with the capacitor C on the right. We obtain for this attenuation factor A_1 ,

$$A_1 = \left| \frac{1}{1 + i\omega C R_J + 1/(i\omega L/R_J + R_S/R_J)} \right|^2, \quad (3)$$

where $R_S = 2R_L + R_S$ and where we have assumed that $R_L \ll 1/\omega C$. The second part A_2 is due to the frequency-dependent gain of the amplifiers. We have carefully measured this dependence in between 1 Hz and 1 MHz and found that the high-frequency roll off can accurately be modeled by a first-order low-pass filter with a crossover frequency of $f_c = 840$ kHz. Hence, A_2 is given by

$$A_2 = \left| \frac{1}{1 + i2\pi f/f_c} \right|^2. \quad (4)$$

All parameters L , R_L , and R_S , and the overall gain can accurately be measured except C . We therefore determine the capacitance C by fitting the frequency dependence of the measured thermal noise $S_V(f)$ to the expected value $4kTR_J A_1(f) A_2(f)$. A consistent *single* value of $C = 270$ pF has been found for different junction resistances. The validity of this calibration procedure is demonstrated in Fig. 2. In Fig. 2(a) the frequency dependence of the measured thermal noise is shown for different metal-film calibration resistances R ranging between 10 Ω and 10 k Ω which were used instead of a real junction. One can see that the f dependence is very strong for large junction resistance values, whereas a flat f -independent part is clearly visible in the opposite case. The expected noise according to $4kTR A_1(f) A_2(f)$ is plotted as dashed curves in Fig. 2(a). A very good agreement with

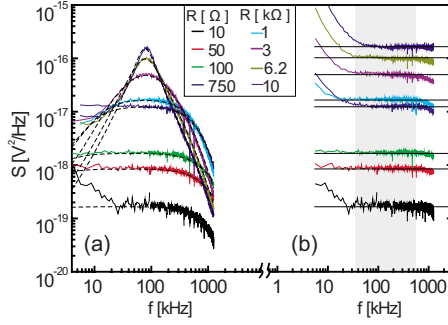


FIG. 2. (Color online) (a) Calibration of the setup by measuring the thermal noise of eight standard metal-film resistors with values R ranging from $10\ \Omega$ to $10\ \text{k}\Omega$. The dashed curves are calculated, taking the frequency dependence of the circuit and gain of the amplifiers into account. In (b) the measured thermal noise is corrected for the known frequency dependence of the circuit and amplifier gains. The horizontal lines mark the theoretical thermal noise of $4kTR$. In the shaded region the corrected noise is frequency independent and coincide with the expected thermal noise values. This frequency interval is used to measure the $1/f$ noise in nanojunctions.

the measured noise is evident. In Fig. 2(b) we display the corrected data, i.e., the measured noise divided by the attenuation factor A . This procedure works very well in the shaded frequency window over the whole resistance range as evidenced by the flat noise plateaus that coincide with the expected thermal noise (horizontal lines). For the $1/f$ noise study we will therefore restrict the frequency window to the shaded region of $30 < f < 400\ \text{kHz}$.

III. RESULTS AND DISCUSSION

Figure 3 shows the f dependence of $S_V(f)$ for a single EM junction in the “low-Ohmic” regime with $R_J = 10\text{--}65\ \Omega$ together with a curve representative for large junction resistances (here, $R_J = 1\ \text{k}\Omega$). To measure $1/f$ noise we typically apply a voltage of $50\ \text{mV}$. This is below the threshold for EM and enables the stable measurements of junctions. Except for the lowest two curves, the main panel of Fig. 3 shows that $S_V(f)$ decays in a power-law fashion but this decay is not exactly inversely proportional to f . This fact has often been noted before: $S_V \propto 1/f^\nu$ with ν ranging between one and two. The latter is expected for a single two-level fluctuator.²⁶ In our case, the exponent ν is close to one with an average of $\nu \approx 1.1$, taking all data with $R_J > 20\ \Omega$. What is remarkable, however, is the sample-to-sample fluctuation in the slope (particularly strongly visible in the $R_J = 40\ \Omega$ curve) which we observe universally in all devices.

In addition to the sample-to-sample fluctuation of the slope around a mean value of $\nu \approx 1.1$, we also see that the bottom curve for the smallest junction resistance of $R_J = 10\ \Omega$ is flat and displays no $1/f$ noise. This is also true for all devices: $1/f$ noise only shows up for a sufficiently large junction resistance R_J and dc bias U_J . This is because the thermal noise of the series connection $R_J + 2R_L$ dominates at a small bias U_J and small R_J . After increasing R_J at constant U_J , the f dependence of S_V sets in. The $1/f$ dependence

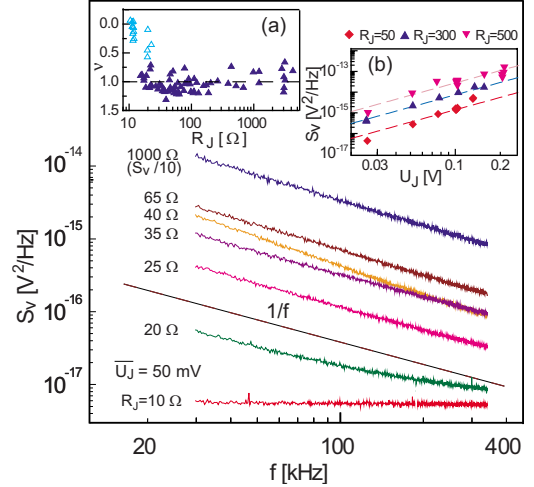


FIG. 3. (Color online) Noise spectra of a single EM junction, measured at $U_J = 50\ \text{mV}$ and for relatively low junction resistances R_J ranging from 10 to $65\ \Omega$ (from bottom to top). For comparison we also show $S_V(f)$ for $R_J = 1\ \text{k}\Omega$. Inset (a): the exponent ν of the frequency dependence deduced from the noise spectrum of many junctions with a large range of junction resistances R_J and bias voltages U_J . The open symbols correspond to devices with small R_J and measurements at small bias voltage U_J , displaying only white noise originating from the lead resistances. The average value of ν for the filled symbols is equal to 1.1 and therefore close to the expected value for $1/f$ noise. The inset (b) shows the bias voltage dependence of S_V at a frequency f of $f_0 = 100\ \text{kHz}$ and for three different R_J values.

shows up first on the low-frequency side. At the high-frequency side the thermal noise still dominates. This leads to the impression that the spectrum is flatter than $1/f$ in this transition regime from low to large R_J values. The deduced power ν in the relation $S_V \propto 1/f^\nu$ is shown in inset (a) of Fig. 3. The open symbols belong to junctions with too low R_J that do not display $1/f$ noise in the given frequency interval and for applied voltage. Only the filled symbols correspond to junctions displaying full $1/f$ noise. There is quite some scatter in ν but all values stay close to $\nu = 1$.

In order to shed light on the origin of the $1/f$ noise, the voltage dependence of S_V has been analyzed. The second inset (b) of Fig. 3 shows S_V taken at a fixed frequency of $100\ \text{kHz}$ as a function of U_J . The different symbols refer to three representative samples with $R_J = 50, 300,$ and $500\ \Omega$. There is a strong increase in S_V with U_J which is in quite good agreement with a quadratic dependence, i.e., $S_V \propto U_J^2$, for not too large voltages ($\leq 0.2\ \text{V}$). This quadratic dependence agrees with our expectation for resistance fluctuations as the source of $1/f$ noise. This expression can be understood by noting that the fluctuating junction resistance δR_J generates the fluctuating voltage $\delta U_J = I \delta R_J$ over the junction at a constant dc bias current I . The mean-square fluctuation, i.e., the noise, is then proportional to I^2 and therefore also to U_J^2 .

Having established the $1/f$ dependence and confirmed resistance fluctuations as its origin, we consider next the prefactor α/N . S_V of many samples has been measured as a function of the junction cross section, i.e., as a function of R_J , and the $1/f$ contribution was extracted within the fre-

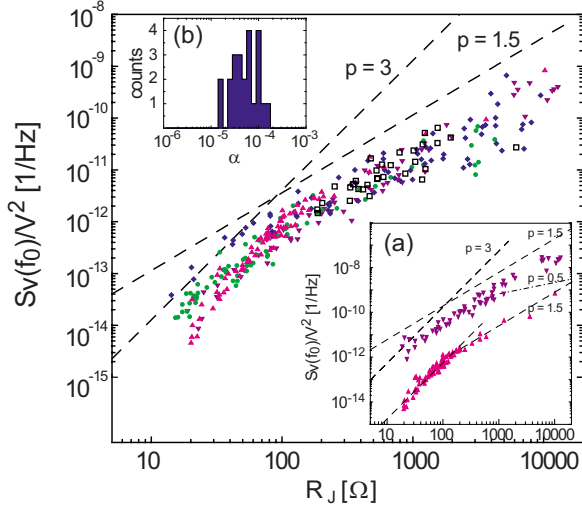


FIG. 4. (Color online) Magnitude of the $1/f$ noise, shown as a log-log scatter plot of $S_V(f_0)/V^2$ with $f_0=100$ kHz of four MCBJ samples and one EM sample (open squares) as a function of junction resistance R_J . The inset (a) shows the data from two MCBJs separately where the upper set is vertically shifted by 2 orders of magnitude for clarity. Dashed lines are guides for the eyes for the expected power-law dependencies $S_V(f_0)/V^2 \propto R_J^p$ in the diffusive ($p=3$) and ballistic ($p=1.5$) regimes. The dashed-dotted line has a slope of $p=0.5$ (see text). The inset (b) shows a histogram of α values deduced from S_V for the single-atom contact when $R_J = h/2e^2$.

quency interval of 30–400 kHz following the procedure described before. To compare the magnitude of S_V for different samples and different junctions, we now take the normalized noise $S_V(f)/V^2$ at a fixed frequency of $f=f_0=100$ kHz.

In Fig. 4 (main panel) we show a scatter plot of $S_V(f_0)/V^2$ as a function of R_J of a few samples in a double-logarithmic representation. Four sets were obtained with MCBJ samples and one with a EM one (open squares). Note that EM samples typically cover only the regime $R_J \geq 100 \Omega$ because, when EM sets in, there is a relatively fast transition from the low-Ohmic regime I in Fig. 1(c) to the intermediate resistance regime II. The scatter plot clearly displays a crossover from a power-law dependence $S_V(f_0)/V^2 \propto R_J^p$ with a large power for low R_J and a smaller one for large R_J . This crossover is better seen in inset (a) of Fig. 4. Although there are some sample-to-sample variations, we always observe a crossover in all of our samples in the vicinity of $R_J \approx 100 \Omega$. The deduced powers are consistent with $p=1.5$ and 3 for large and low R_J , respectively. The transition and the deduced values are in agreement with $1/f$ noise generated in the bulk together with a transition from the diffusive to the ballistic transport regime with increasing R_J as we will outline in the following.

It has been pointed out by Hooge⁴² that $1/f$ noise is a bulk phenomenon, whose scaling parameter N [see Eq. (1)] should grow like the volume Θ . Although this has been disputed and was discussed many times over the last two decades, we will assume scaling with volume and compare to scaling with the surface afterwards. Let us denote a characteristic length of the junction by l . In order to refer to size

scaling, we use the terminology length $\sim l$, which reads “length scales with l .” Obviously, $\Theta \sim l^3$. In a diffusive wire of length L and cross section A , the resistance R is given by $R = \rho L/A$, where ρ is the specific resistance. Hence, $R \sim l^{-1}$. Because $S_V/V^2 \propto 1/N \sim l^{-3}$ [Eq. (1)], we expect $S_V/V^2 \propto R^3$ in this transport regime. If the characteristic length of the junction becomes shorter than the momentum scattering mean-free path, one is entering the ballistic regime. In this regime, the conductance is determined by the number of transport channels which is proportional to the junction area. The corresponding junction resistance is the so-called Sharvin resistance.⁵⁵ Hence, $R \propto A^{-1} \sim l^{-2}$. Consequently, $S_V/V^2 \propto R^{1.5}$. The data in Fig. 4 show a crossover which agrees with these derived exponents.

As a comparison, we also derive the expected power if transport is ballistic and the fluctuators leading to $1/f$ noise are only present on the surface. All transport channels in the interior of the junction are assumed to be noiseless. Now, S_V/V^2 will be inversely proportional to N_S , where N_S stands for the number of transport channels on the surface. This number scales as the circumference, and therefore $N_S \sim l$. Using the Sharvin resistance for a ballistic contact $R \propto A^{-1} \sim l^{-2}$, we arrive at $S_V/V^2 \propto R^{1/2}$. This value for p is considerably smaller than $p=1.5$. In inset (a) of Fig. 4 the dash-dotted line corresponds to $p=0.5$. It is clear that the slope of the measured data points is larger proving that even in small metallic junctions, in which only a few channels carry the charge current, all of them contribute to $1/f$ noise and not only the channels close to the surface.

Finally, we can estimate the parameter α in Eq. (1). This parameter corresponds to the noise value for $N=1$ at $f=1$ Hz. If we associate with N the number of electrons (which for Au is the same as the number of atoms), we have to look at the S_V value for the single-atom contact. Because R_J is then given by the quantum resistance $h/2e^2 \approx 13$ k Ω , we find from Fig. 4 $S_V(f_0)/V^2 \approx 10^{-10} - 10^{-9}$ Hz⁻¹. Multiplying with $f_0=100$ kHz yields $\alpha \approx 10^{-5} - 10^{-4}$. α values deduced in this way are shown as a histogram in inset (b) of Fig. 4. This range of α values compares very well with parameters reported in the literature.²⁶ This is quite remarkable because, unlike the measurements on large conductors, we identify with the number of independent fluctuators N in Eq. (1) the number of atoms. This is usually not justified. In a single crystal with a very low defect density, for example, N will not be determined by the number of atoms but rather by the number of defects. The reason why we deduced Hooge parameters that agree with literature values in our approach suggests that the effective scattering length scales with the size of the junction down to the atomic scale. But this is what we must expect for an atomically confined junction.

IV. CONCLUSIONS

In conclusion, we have studied $1/f$ noise at room temperature in tunable electromigration and mechanical controllable break junctions made from Au in a regime in which only a few number of transport channels (1–1000) contribute to the overall conductance. The transition from the diffusive to the ballistic transport regime is clearly visible in the nor-

malized noise S_V/V^2 when plotted against the junction resistance R_J . This transition appears at $R_J \approx 100 \Omega$. We find that even in the smallest junctions, $1/f$ noise scales with the total number of channels in the “bulk” (cross section).

ACKNOWLEDGMENT

This work has been supported by the Swiss National Center (NCCR) on Nanoscale Science, the Swiss National Science Foundation, and the University of Basel.

*christian.schoenenberger@unibas.ch

- ¹P. Bak, C. Tang, and K. Wiesenfeld, Phys. Rev. Lett. **59**, 381 (1987).
- ²A. van der Ziel, *Noise* (Prentice-Hall, Englewood Cliffs, 1954).
- ³Sh. Kogan, *Electronic Noise and Fluctuations in Solids* (Cambridge University Press, Cambridge, 1996).
- ⁴Ya. M. Blanter and M. Büttiker, Phys. Rep. **336**, 1 (2000).
- ⁵C. Beenakker and C. Schönberger, Phys. Today **56** (5), 37 (2003).
- ⁶J. B. Johnson, Phys. Rev. **32**, 97 (1928).
- ⁷H. Nyquist, Phys. Rev. **32**, 110 (1928).
- ⁸W. Schottky, Ann. Phys. **362**, 541 (1918).
- ⁹F. N. Hooge, Phys. Lett. **29**, 139 (1969).
- ¹⁰R. F. Voss and J. Clarke, Phys. Rev. B **13**, 556 (1976).
- ¹¹D. A. Bell, J. Phys. C **13**, 4425 (1980).
- ¹²F. N. Hooge, T. G. M. Kleinpenning, and L. K. J. Vandamme, Rep. Prog. Phys. **44**, 479 (1981).
- ¹³P. Dutta and P. M. Horn, Rev. Mod. Phys. **53**, 497 (1981).
- ¹⁴M. S. Keshner, Proc. IEEE **70**, 212 (1982).
- ¹⁵D. M. Fleetwood, J. T. Masden, and N. Giordano, Phys. Rev. Lett. **50**, 450 (1983).
- ¹⁶N. Giordano, Rev. Solid State Sci. **3**, 27 (1989).
- ¹⁷M. B. Weissman, Rev. Mod. Phys. **60**, 537 (1988).
- ¹⁸L. K. J. Vandamme, Xiasong Li, and D. Rigaud, IEEE Trans. Electron Devices **41**, 1936 (1994).
- ¹⁹R. S. Sorbello, in *Materials Reliability Issues in Microelectronics*, edited by J. R. Lloyd, F. G. Yost, and P. S. Ho, MRS Symposia Proceedings No. 225 (Materials Research Society, Warrendale, 1991), pp. 3–13.
- ²⁰L. K. J. Vandamme, IEEE Trans. Electron Devices **41**, 2176 (1994).
- ²¹K. Dagge, W. Frank, A. Seeger, and H. Stoll, Appl. Phys. Lett. **68**, 1198 (1996).
- ²²J. Dong and B. A. Parviz, Nanotechnology **17**, 5124 (2006).
- ²³I. K. Yanson, A. I. Akimenko, and A. B. Verkin, Solid State Commun. **43**, 765 (1982).
- ²⁴A. I. Akimenko, A. B. Verkin, and I. K. Yanson, J. Low Temp. Phys. **54**, 247 (1984).
- ²⁵K. S. Ralls and R. A. Buhrman, Phys. Rev. B **44**, 5800 (1991).
- ²⁶P. A. M. Holweg, J. Caro, A. H. Verbruggen, and S. Radelaar, Phys. Rev. B **45**, 9311 (1992).
- ²⁷G. Zimmerli, T. M. Eiles, R. L. Kautz, and J. M. Martinis, Appl. Phys. Lett. **61**, 237 (1992).
- ²⁸H. Birk, M. J. M. de Jong, and C. Schönberger, Phys. Rev. Lett. **75**, 1610 (1995).
- ²⁹F. Liefink, A. J. Scholten, C. Dekker, J. I. Dijkhuis, B. W. Alphenaar, H. van Houten, and C. T. Foxon, Phys. Rev. B **46**, 15523 (1992).
- ³⁰B. Neri, C. Ciofi, and V. Dattilo, IEEE Trans. Electron Devices **44**, 1454 (1997).
- ³¹A. Bid, A. Bora, and A. K. Raychaudhuri, Phys. Rev. B **72**, 113415 (2005).
- ³²N. O. Birge, B. Golding, and W. H. Haemmerle, Phys. Rev. Lett. **62**, 195 (1989).
- ³³C. Strunk, M. Henny, C. Schönberger, G. Neuttiens, and C. Van Haesendonck, Phys. Rev. Lett. **81**, 2982 (1998).
- ³⁴D. Hoadley, P. McConville, and N. O. Birge, Phys. Rev. B **60**, 5617 (1999).
- ³⁵G. Neuttiens, C. Strunk, C. Van Haesendonck, and Y. Bruynseraede, Phys. Rev. B **62**, 3905 (2000).
- ³⁶P. G. Collins, M. S. Fuhrer, and A. Zettl, Appl. Phys. Lett. **76**, 894 (2000).
- ³⁷E. S. Snow, J. P. Novak, M. D. Lay, and F. K. Perkins, Appl. Phys. Lett. **85**, 4172 (2004).
- ³⁸M. Ishigami, J. H. Chen, E. D. Williams, D. Tobias, Y. F. Chen, and M. S. Fuhrer, Appl. Phys. Lett. **88**, 203116 (2006).
- ³⁹E. Onac, F. Balestro, B. Trauzettel, C. F. J. Lodewijk, and L. P. Kouwenhoven, Phys. Rev. Lett. **96**, 026803 (2006).
- ⁴⁰R. Möller, A. Esslinger, and B. Koslowski, Appl. Phys. Lett. **55**, 2360 (1989).
- ⁴¹Xiuguang Jiang, M. A. Dubson, and J. C. Garland, Phys. Rev. B **42**, 5427 (1990).
- ⁴²F. N. Hooge, Physica B **162**, 344 (1990).
- ⁴³M. Tacano, IEEE Trans. Electron Devices **40**, 2060 (1993).
- ⁴⁴E. P. Vandamme and L. K. J. Vandamme, IEEE Trans. Electron Devices **47**, 2146 (2000).
- ⁴⁵C. T. Sah and F. Hielscher, Phys. Rev. Lett. **17**, 956 (1966).
- ⁴⁶L. K. J. Vandamme, IEEE Trans. Electron Devices **36**, 987 (1989).
- ⁴⁷H. Wong, Y. C. Chng, and G. Ruan, J. Appl. Phys. **67**, 312 (1990).
- ⁴⁸H. Park, A. K. L. Lim, J. Park, A. P. Alivisatos, and P. L. McEuen, Appl. Phys. Lett. **75**, 301 (1999).
- ⁴⁹J. M. van Ruitenbeek, A. Alvarez, I. Pineyro, C. Grahmann, P. Joyez, M. H. Devoret, D. Esteve, and C. Urbina, Rev. Sci. Instrum. **67**, 108 (1996).
- ⁵⁰E. Scheer, P. Joyez, D. Esteve, C. Urbina, and M. H. Devoret, Phys. Rev. Lett. **78**, 3535 (1997).
- ⁵¹N. Agrait, A. L. Yeyati, and J. M. van Ruitenbeek, Phys. Rep. **377**, 81 (2003).
- ⁵²Zheng Ming Wu, M. Steinacher, R. Huber, M. Calame, S. J. van der Molen, and C. Schönberger, Appl. Phys. Lett. **91**, 053118 (2007).
- ⁵³L. Grüter, M. T. Gonzalez, R. Huber, M. Calame, and C. Schönberger, Small **1**, 1067 (2005).
- ⁵⁴M. L. Trouwborst, S. J. van der Molen, and B. J. van Wees, J. Appl. Phys. **99**, 114316 (2006).
- ⁵⁵Y. V. Sharvin, Sov. Phys. JETP **21**, 655 (1965).